ECHAHID HAMMA LAKHDAR UNIVERSITY - EL-OUED
Under the Supervision of the DGRSDT and in collaboration with the CRTI
International Pluridisciplinary PhD Meeting (IPPM'20)
23-26, 2020 1st Edition, February
Theme: Modern Technology and Fineness Life

4 to 5 pages

A Hybrid Intelligent Control of A Doubly Fed Asynchronous Generator in Wind Turbine

Abdelhafid Guediri*, Abdelkarim Guediri* , zakaria Lammouchi *

* Electric engineering department, LABO Laboratory, El-Oued University, Algeria
E-mail: toufikguediri1@gmail.com,karim_elect @ yahoo.fr, prof_lammouchi@yahoo.fr

Abstract

This paper presents an A Hybrid Intelligent control of a doubly fed asynchronous machine (DFAM) is proposed. First, a mathematical model of DFAM written in an appropriate d-q reference frame is established to investigate simulations results. and to maintain the constant voltage of the DC link. Performance is also tested in different situations. In order to control the rotary currents from DFAM, the torque tracking control law is manufactured using PI controllers; the stator side power factor is controlled at unity level. Specifically neuro-fuzzy systems are created to overcome the disadvantages of neural networks and The effectiveness of the proposed control strategy is evaluated under different operating conditions such as reference speed and torque step changes at nominal parameters and in the presence of a difference in the parameter. Simulation results show that the mysterious logical console is stronger than the traditional IP console in the face of differing parameters and uncertainty, and is less sensitive to torque disturbance in external load with a rapid dynamic response; Its simulated displays are then compared to the performance of the classic PI controller.

Keywords: Turbine; Doubly fed asynchronous machine (DFAM) ; neuro-fuzzy control.

1. Introduction

Doubly-Fed Asynchronous is an electrical asynchronous three-phases Three periods asynchronous machine with open rotor windings which can be fed by external voltages. Fixed windings are connected directly to the line network, while the rotating windings are controlled by an inverter. This solution is very attractive for all applications where there are limited speed differences around the synchronous speed, because the power at which the converter handles the rotor side will be part (according to the slip) of overall system power,[1][2]. Under optimal control conditions, the variable speed wind system can extract a maximum wind power for a wide range of wind [3]. The anemometers are used to measure the wind speed and derive the desired optimal speed turbine command.

2. WIND TURBINE MODEL

Several models for power production capability of wind turbines have been developed. The mechanical power, captured P_{mech} by a wind turbine, depends on its power coefficient Cp given for a wind velocity and can be represented by

$$P_{mech}= \frac{1}{2} C_P \rho \pi R^2 V^3 \quad (1)$$

Where **ρ** and **R** correspond to the air density and the radius of the turbine propeller, respectively [6]. In order to extract the maximum power of the incident wind, permanently must adjust the rotational speed of the turbine to the wind. DFIG speed is used as the reference value for the integrated proportional control unit type (PI lead) as shown in the following figure:

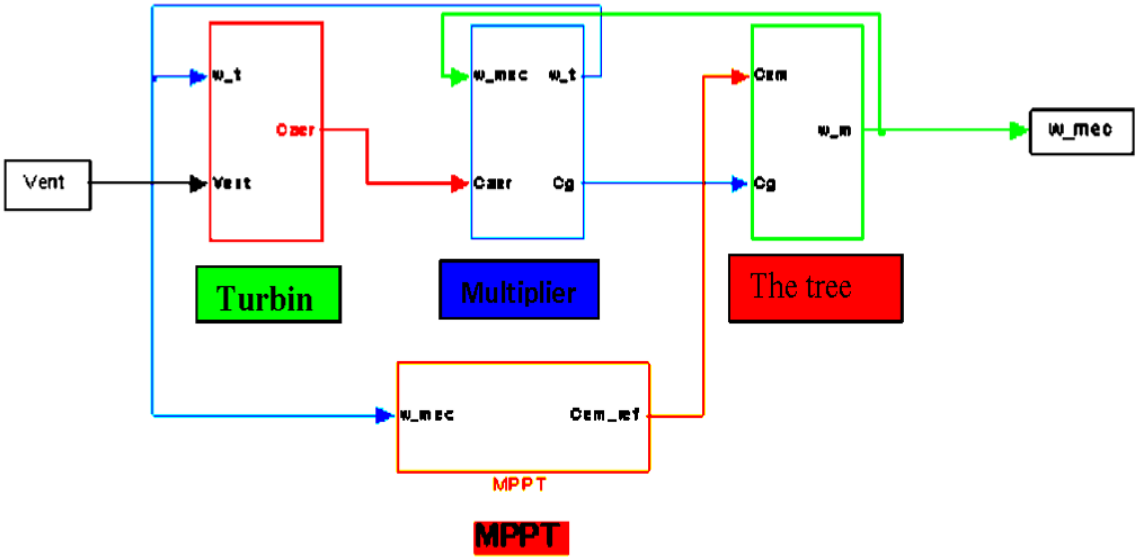

Figure 1: Block diagram of maximizing the power extracted with speed control

The power factor Cp is generally defined as a function of the edge velocity ratio, which in turn is given by λ

$$\lambda = \frac{wR}{V} \qquad (2)$$

It represents the rotational speed of the wind turbine. Shows a typical relationship between the power factor Cp and the edge velocity ratio. The indication indicates that there is a value to ensure the maximum of

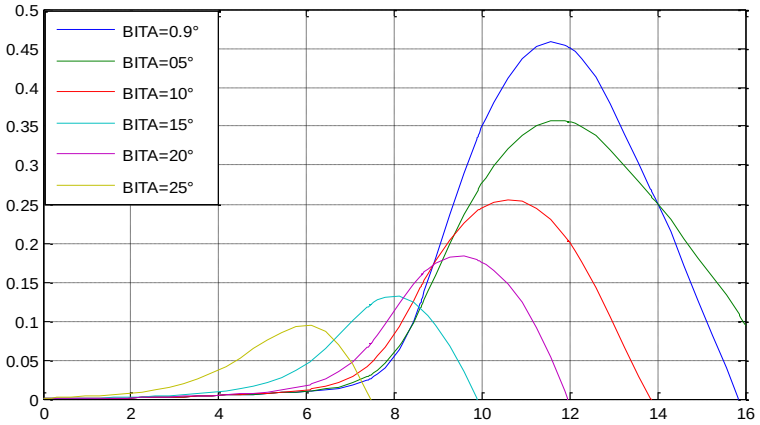

Figure 2: Typical Power Coefficient Versus Tip-Speed-Ratio Curve.

3. DYNAMIC SIMULATION OF DFIG IN TERMS OF DQ - WINDINGS

The dynamic performance of ac machine is somewhat complex because the three phase rotor windings move with respect to three phase stator windings. The analysis can be simplified greatly by transforming the three phase stator and rotor windings to a factious two phase stator and rotor. These fictions two phase windings are called d-q windings[4]. The stator and rotor a-, b- and c-phase voltage equations can be transformed to the d-q axis. Then the generator electrical model is derived from the following equations.

$$\begin{cases} V_{sd} = R_s I_{sd} + \frac{d\varphi_{sd}}{dt} - \omega_s \varphi_{sq} \\ V_{sq} = R_s I_{sq} + \frac{d\varphi_{sq}}{dt} + \omega_s \varphi_{sd} \\ V_{rd} = R_r I_{rd} + \frac{d\varphi_{rd}}{dt} - (\omega_s - \omega)\varphi_{rq} \\ V_{rq} = R_r I_{rq} + \frac{d\varphi_{rq}}{dt} + (\omega_s - \omega)\varphi_{rd} \\ T_e = \frac{3}{2} pM\left(I_{sq} I_{rd} - I_{sd} I_{rq}\right) \end{cases} \quad (3)$$

4. ACTIVE AND REACTIVE POWER CONTROL OF DFIG

The active and reactive powers are found by using the Equations as below.

$$\begin{cases} \text{Ps} = -\text{V}_s \frac{M}{L_s} . I_{rq} \\ Q_s = \frac{\text{V}_s . \varphi_s}{L_s} - \frac{\text{V}_s M}{L_s} I_{rd} \\ P_r = g\text{V}_s \frac{M}{L_s} . I_{rq} \\ Q_r = g\text{V}_s \frac{M}{L_s} . I_{rd} \end{cases} \quad (4)$$

5. CONTROL STRATEGY

The control strategy of the RSC and GSC consists of an "active and reactive power" controlling outer loop and the "current control" inner loop. [5]

The control principle of the rotor side converter (RSC) allows the control of active and reactive power and the extraction of maximum wind power as shown in **Fig. 3**

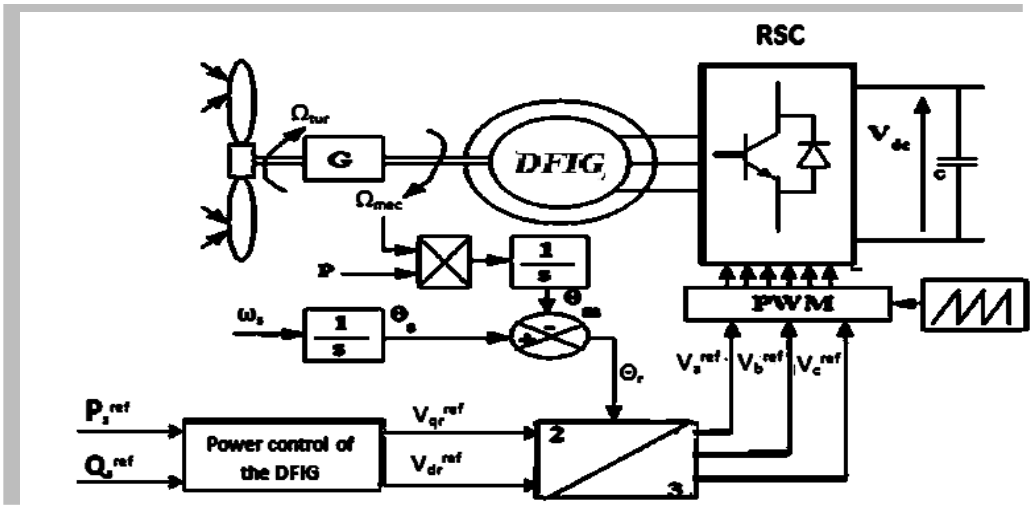

Figure 3: Control Structure of Rotor Side Converter.

The reference interactive power can be set to zero to operate the unit power factor.

Express the current q-axis reference as it is

$$I_{gqref} = [K_{PP} + \frac{K_{iP}}{S}](P_{ref} - P_{grid}) \quad (5)$$

Where K_{pp} *and* K_{ip} are proportional and integral constants of the grid power regulator respectively. The expressions for the control voltages in the d-q frame are given as

$$V_{dgsc} = [K_{pgsc} + \frac{K_{igsc}}{S}](i_{gdref} - i_{gd}) \quad (6)$$

$$V_{qgsc} = [K_{pgsc} + \frac{K_{igsc}}{S}](i_{gqref} - i_{gq}) \quad (7)$$

Where igd and igq are the sensed d-q components of the grid currents respectively.

6. DESIGN OF THE NEURO-FUZZY CONTROLLER

Fig.4 shows the block diagram of the neuro-fuzzy controller (NFC) system. The NFC controller is composed of an on-line learning algorithm with a neuro-fuzzy network. The neuro-fuzzy network is trained using an on-line learning algorithm[11].

6.1 Description of NFC:

For the NFC, a four layer NN as shown in Fig. 5 is used. Layers *I–IV* represents the inputs of the network, the membership functions, the fuzzy rule base and the outputs of the network, respectively.

6.1.1 Layer I: input layer

Inputs and outputs of nodes in this layer are represented as:

$$net_1^I = e_{idr}(t), y_1^I = f_1^I(net_1^I) = net_1^I = e_{idr}(t) \quad (15)(8)$$

$$net_2^I = \delta e_{idr}(t), y_2^I = f_1^I(net_1^I) = net_1^I = \delta e_{idr}(t) \quad (16)(9)$$

Where $e_{idr} and\ \delta e_{idr} inputs\ are y_1^I\ and\ y_2^I$ are outputs of the input layer. In this layer, the weights are unity and fixed.

6.1.2 Layer II: Membership layer

In this layer, each node performs a fuzzy set and the Gaussian function is adopted as a membership function

$$net_{1.j}^{II} = -\frac{\left(x_{1.j}^{II} - m_{1.j}^{II}\right)^2}{\left(\delta_{1.j}^{II}\right)^2}, y_{1.j}^{II} = f_{1.j}^{II}\left(net_{1.j}^{II}\right) = exp\left(net_{1.j}^{II}\right) \quad (17)\ (10)$$

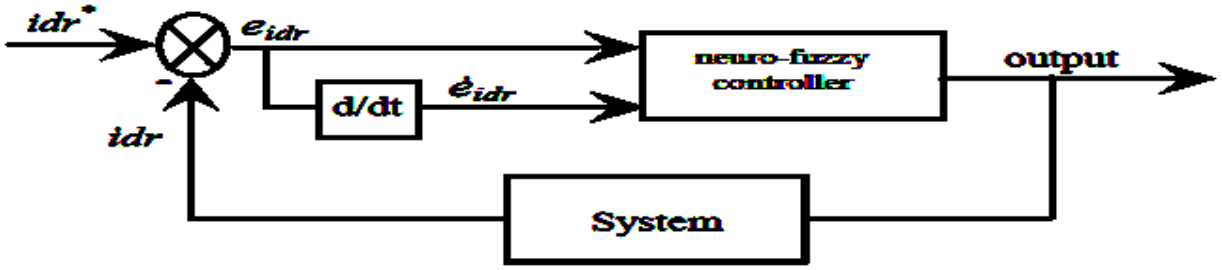

Figure 4: Block diagram of the neuro-fuzzy controller

$$net_{2.k}^{II} = -\frac{\left(x_{2.j}^{II} - m_{2.j}^{II}\right)^2}{\left(\delta_{2.k}^{II}\right)^2}, y_{2.k}^{II} = f_{2.k}^{II}(net_{2.k}^{II}) = exp(net_{2.k}^{II}) \quad (18) \quad (11)$$

Where: $m_{1.j}^{II}\ m_{2.k}^{II}\ and\ \delta_{1.j}^{II}, \delta_{2.k}^{II}$ are, respectively, the mean and the standard deviation of the Gaussian function. There are $j + k$ nodes in this layer[10].

6.1.3 Layer III: Rule layer

This layer includes the rule base used in the fuzzy logic control (FLC). Each node in this layer multiplies the input signals and outputs the result of product

$$net_{j,k}^{III} = \left(x_{1,j}^{III} \times x_{2,k}^{III}\right), y_{jk}^{III} = f_{jk}^{III}\left(net_{jk}^{III}\right) = net_{jk}^{III} \quad (19)(12)$$

6.1.4 Layer IV: Output layer

This layer represents the inference and defuzzification used in the FLC. For defuzzification, the center of area method is used; therefore the following form can be obtain:

$$a = \sum_j \sum_k w_{jk}^{IV}\, y_{jk}^{III}, b = \sum_j \sum_k y_{jk}^{III} \quad (20)(13)$$

$$net_0^{IV} = \frac{a}{b}, y_0^{IV} = f_0^{IV}(net_0^{IV}) = \frac{a}{b} \quad (21)\ (14)$$

Where y_{jk}^{III} is the output of the rule layer; a and b are the numerator and the denominator of the function used in the center of area method, w_{jk}^{IV} is the center of the output The aim of the learning algorithm is to adjust the weights of membership functions used in the FLC, respectively[12].

$w_{jk}^{IV}, m_{1.j}^{II}\ m_{2.k}^{II}\ ,\ \delta_{1.j}^{II}\ , \delta_{2.k}^{II}$ .The on-line learning algorithm is a gradient descent search algorithm in the space of network parameters.

$$\delta_0^{IV} = -\frac{\delta e_{idr}(t)\, \dot{e_{idr}}(t)}{\delta y_0^{IV}} \frac{\delta y_0^{IV}}{net_0^{IV}} = \mu_5 e_{idr}(t) \qquad (22)(15)$$

Where μ_5 is the learning-rate for w_{jk}^{IV} and it can be shown in following equation. Therefore, the changing of w_{jk}^{IV} is written as [13]:

$$\Delta w_{jk}^{IV} = -\frac{\partial e_{idr}(t)\, \dot{e_{idr}}(t)}{\partial net_0^{IV}} \frac{\partial net_0^{IV}}{\partial a} \frac{\partial a}{\partial w_{jk}^{IV}} = \frac{1}{b}\ \delta_0^{IV}\ y_{jk}^{III} \qquad (23)(16)$$

Since the weights in the rule layer are unified, only the approximated error term needs to be calculated and propagated by the following equation:

$$\delta_0^{IV} = -\frac{\partial e_{idr}(t)\, \dot{e_{idr}}(t)}{\partial net_0^{IV}} \frac{\partial net_0^{IV}}{\partial y_{1,j}^{III}} \frac{\partial y_{1,j}^{III}}{\partial net_{jk}^{III}} = \frac{1}{b}\ \delta_0^{IV}\ \left(w_{jk}^{IV} - y_0^{IV}\right) \qquad (24)(17)$$

The error received from Layer III is computed as:

$$\delta_{1k}^{II} = \sum_k \left[\left(-\frac{\partial e_{idr}(t)\, \dot{e_{idr}}(t)}{\partial net_{jk}^{III}}\right) \frac{\partial net_{jk}^{III}}{\partial y_{1,j}^{II}} \frac{\partial y_{1,j}^{II}}{\partial net_{1j}^{II}}\right] = \sum_k \delta_{jk}^{III} y_{jk}^{III} \qquad (25)(18)$$

$$\delta_{2k}^{II} = \sum_j \left[\left(-\frac{\partial e_{idr}(t)\, \dot{e_{idr}}(t)}{\partial net_{jk}^{III}}\right) \frac{\partial net_{jk}^{III}}{\partial y_{2,k}^{II}} \frac{\partial y_{2,k}^{II}}{\partial net_{2,k}^{II}}\right] = \sum_j \delta_{jk}^{III} y_{jk}^{III} \qquad (26)(19)$$

The updated laws of $m_{1.j}^{II}\ m_{2.k}^{II}\ and\ \delta_{1.j}^{II}\ , \delta_{2.k}^{II}$ also can be obtained by the gradient decent search algorithm[13]

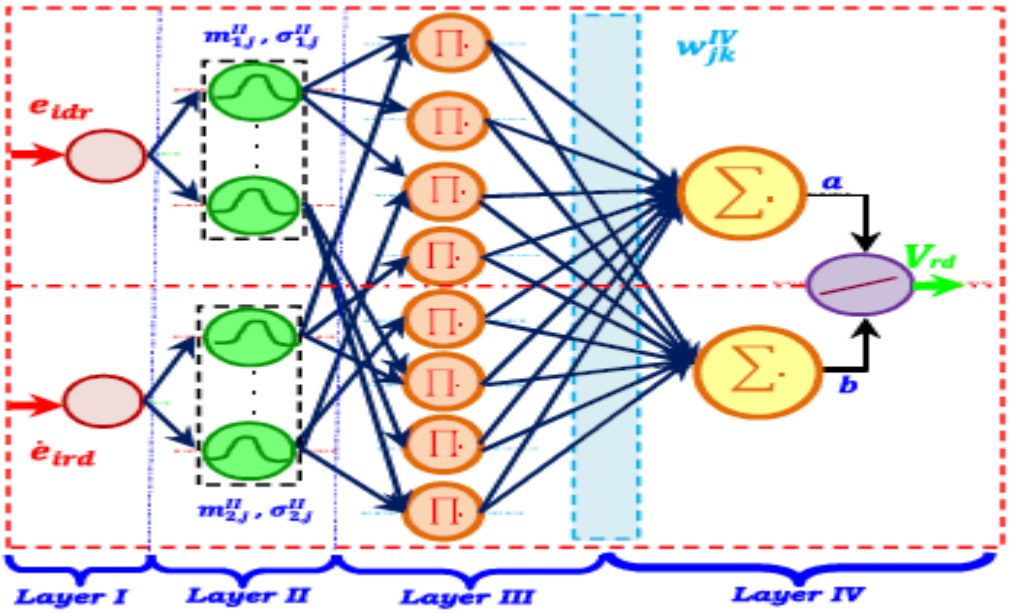

Figure 5: Schematic diagram of the neuro-fuzzy network

$$\Delta m_{1.j}^{II} = -\frac{\partial e_{idr}(t)\, \dot{e_{idr}}(t)}{\partial net_{1.j}^{II}} \frac{\partial net_{1.j}^{II}}{\partial m_{1,j}^{II}} = \mu_4\, \delta_{1.j}^{II}\, \frac{2\left(x_{1.j}^{II} - m_{1.j}^{II}\right)}{\left(\delta_{1.j}^{II}\right)^2} \qquad (27)\ (20)$$

$$\Delta m_{2k}^{II} = -\frac{\partial e_{idr}(t)\, \dot{e_{idr}}(t)}{\partial net_{2.k}^{II}} \frac{\partial net_{2.k}^{II}}{\partial m_{2.k}^{II}} = \mu_4\, \delta_{2.k}^{II}\, \frac{2\left(x_{2.k}^{II} - m_{2.k}^{II}\right)}{\left(\delta_{2.k}^{II}\right)^2} \qquad (28)(21)$$

$$\Delta \delta_{1.j}^{II} = -\frac{\partial e_{idr}(t)\, \dot{e_{idr}}(t)}{\partial net_{1.j}^{II}} \frac{\partial net_{1.j}^{II}}{\partial \delta_{1,j}^{II}} = \mu_2\, \delta_{1.j}^{II}\, \frac{2\left(x_{1.j}^{II} - m_{1.j}^{II}\right)}{\left(\delta_{1.j}^{II}\right)^3} \qquad (29)\ \ (22)$$

Where $\mu_4, \mu_3, \mu_2\ and\ \mu_1$ are the learning-rate parameters of the mean and the standard deviation of the Gaussian functions

7. SIMULATION RESULTS

Fig. 6 shows the block diagram of the DFIG neuro-fuzzy. The results. **Fig.7** shows the results of rotor currents responses using neuro-fuzzy, respectively. The stator power Ps follows the current I_{rq}. These results in unity power factor on the grid as the stator reactive power Qs is zero are shown in **Fig.8**. Rotor current errors are controlled at zero level. The reactive component of the stator current I_{sd} is almost equal to zero during all the timeas shown in **Fig. 9**. As result, the stator phase current, reported in **Fig.10**, has an opposite phase angle to the line voltage indicating that the stator power is injected to the line grid. Reported in **Fig.11**and **Fig.14**, shows the results of stator and rotor three Phase currents responses using neuro-fuzzy.

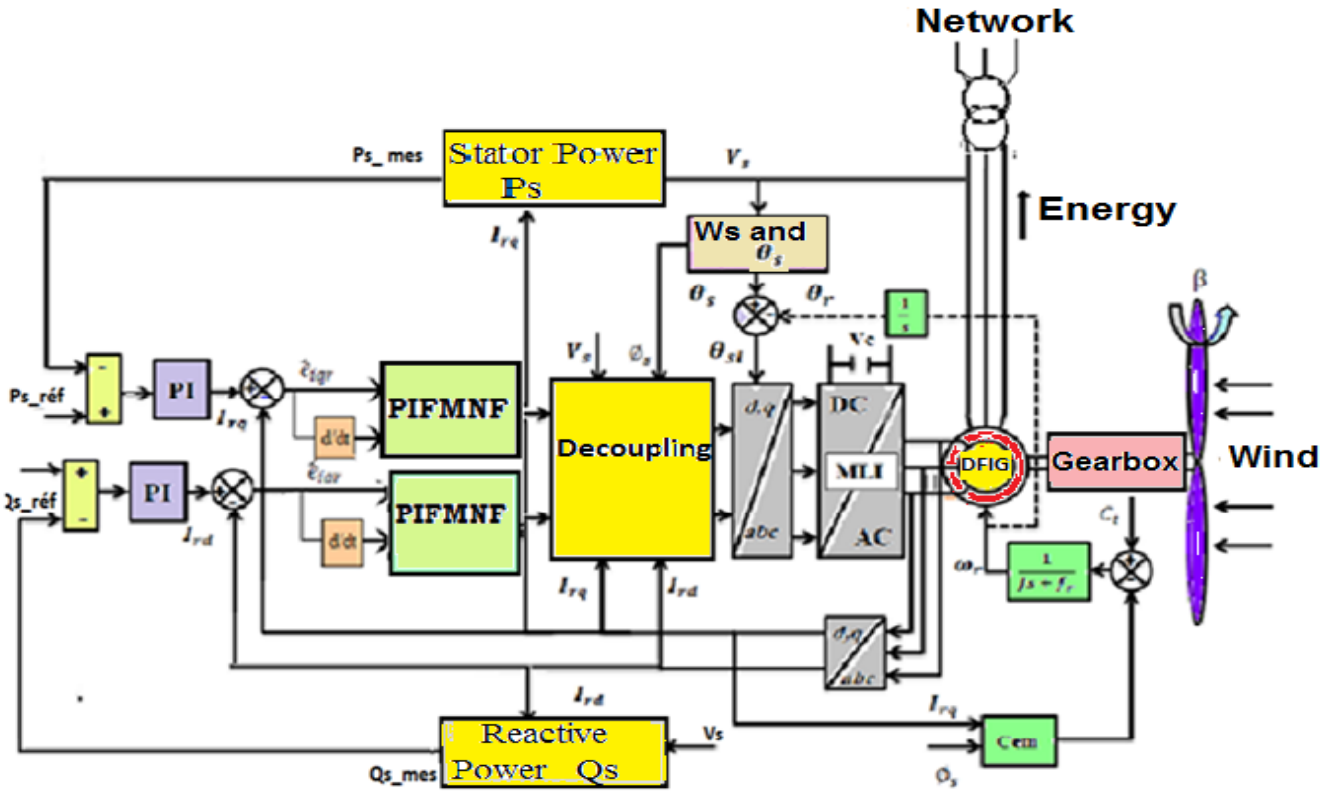

Figure 6: Block diagram of the DFIG neuro-fuzzy

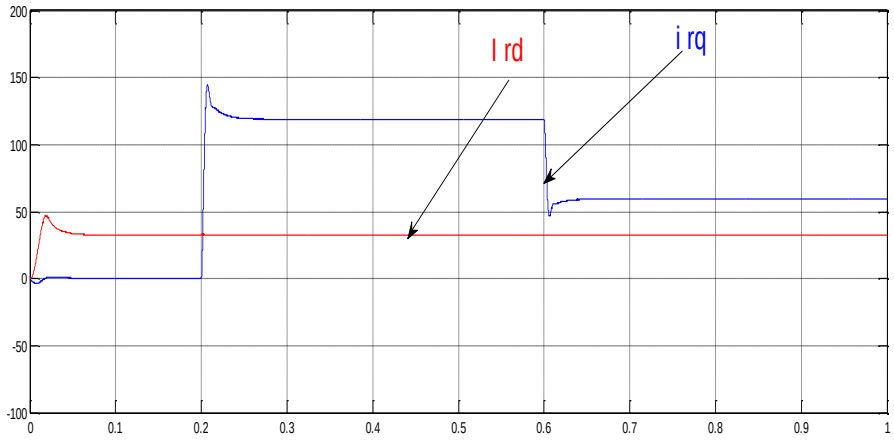

Figure 7: Rotor currents responses

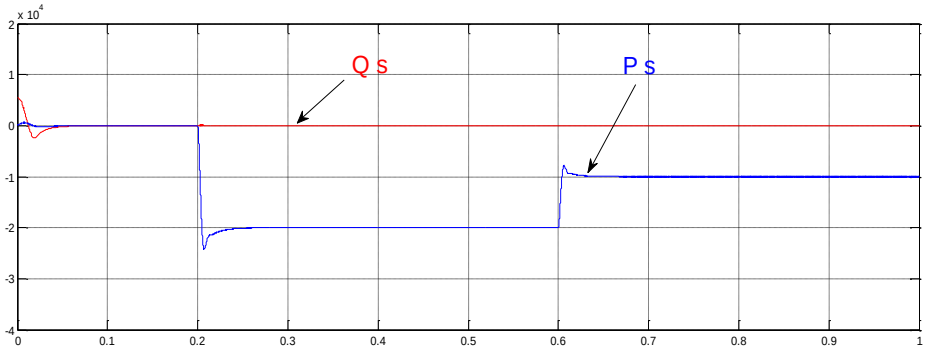

Figure 8: Active and reactive powers

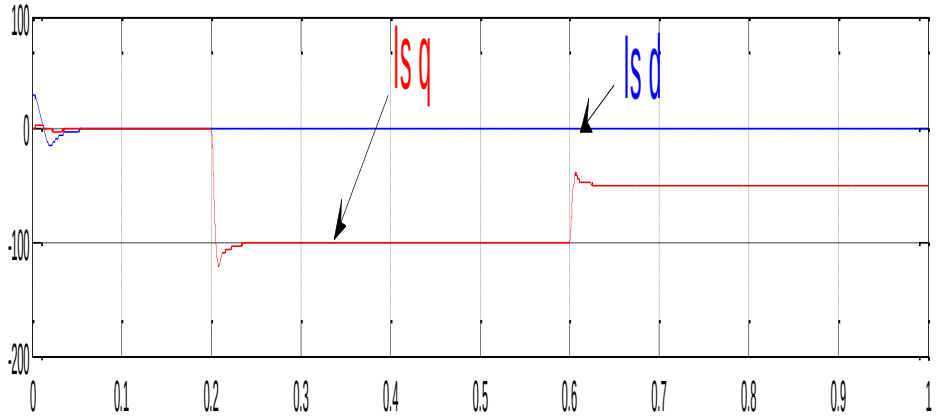

Figure 9: Stator currents response With neuro-fuzzy

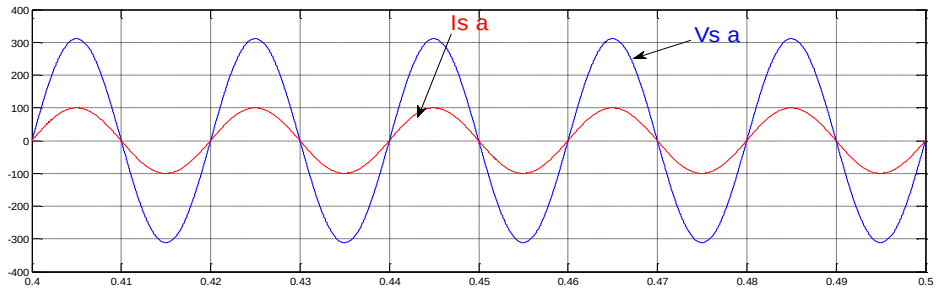

Figure 10: Stator voltage and current

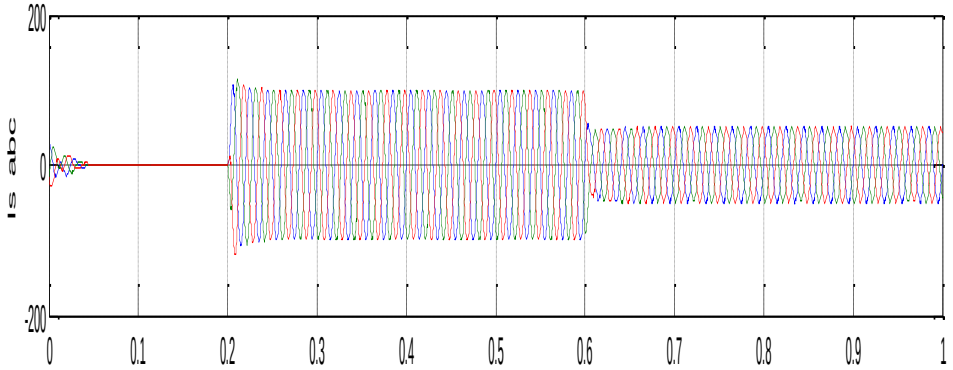

Figure 11: Stator Three Phase Currents (Is_ abc).

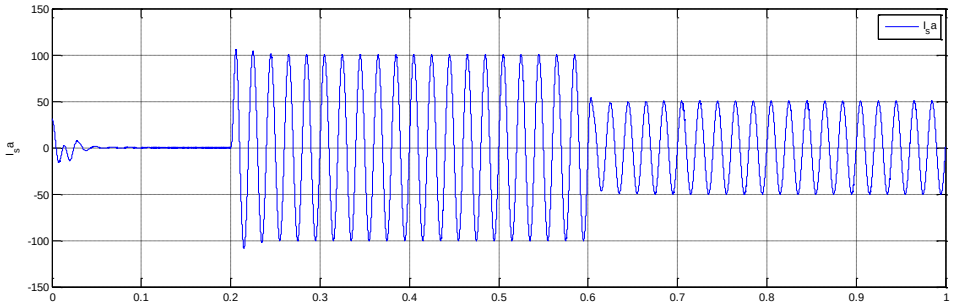

Figure 12: Stator per phase Currents (Is_ a)

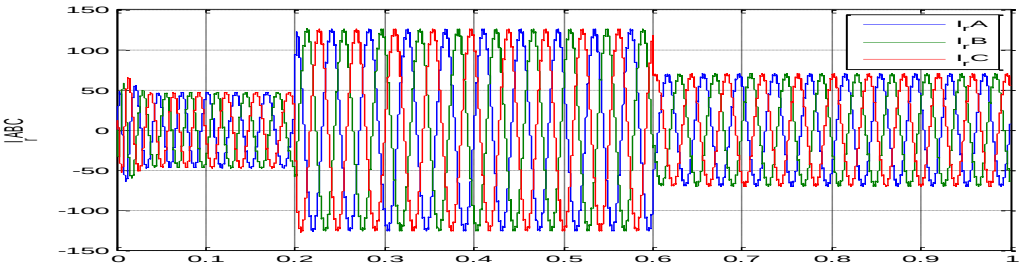

Figure 13: Rotor Three Phase Currents (Ir_ abc).

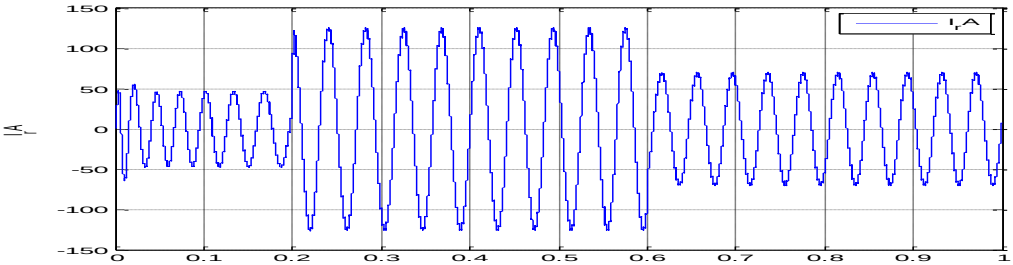

Figure 14: phase Rotor Currents (Ir_ a).

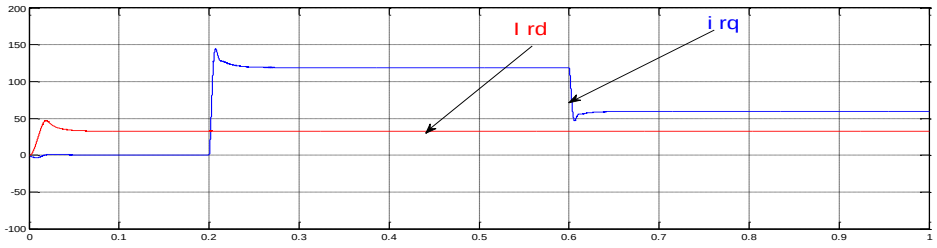

Figure 15: Rotor currents responses to With neuro-fuzzy parameters variations

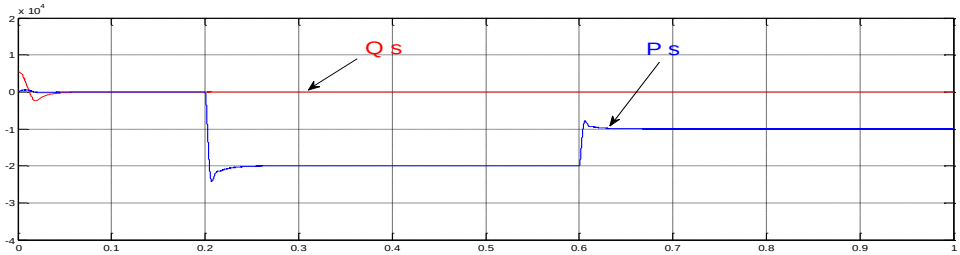

Figure 16: Active and reactive powers responses to parameters variations With neuro-fuzzy

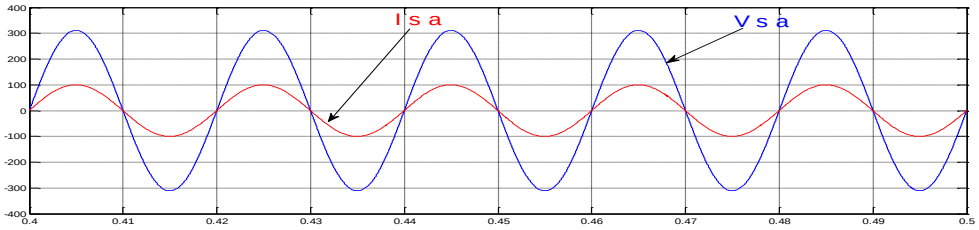

Figure 17: Stator voltage and current responses to parameters variations With neuro-fuzzy

8. CONCLUSION

In this paper a hybrid intelligent control based torque tacking approach for doubly fed asynchronous drive have been proposed. Torque tracking control strategy has been achieved by adjusting the rotating currents and using the reference frame guide for the constant voltage vector. The performance of the nerve valve control unit based on the torque tracking algorithm was checked and compared with the performance obtained from the PI controller.

Simulations results have shown that the NFC is more robust, efficient and more robust under parameters variations of the DFIG.

ANNEXURE

TURBINE PARAMETERS

Baled radius,	R= 35.25m
Number of blades	N=3
Gearbox ratio,	G= 90
Moment of inertia,	J= 1000 Kg.m^2
Viscous friction coefficient,	f =0.0024 N.m.s^{-1}
Cut-in wind speed	4 m/s
Cut-out wind speed	25 m/s
Nominal wind speed,	v= 16 m/s

Wound Rotor Induction Machine Parameters:-

Nominal Power	Pn = 1.5 MW
Stator Voltage	vs = 200V
Stator Frequency	fs = 50 Hz
Stator Resistance	Rs = 0.12 Ω
Stator Inductance	Ls = 0.0205 H
Rotor Resistance	Rr = 0.021 Ω
Rotor Inductance	Lr = 0.0204H
Mutual Inductance	Lm = 0.0169 H
Inertia Constant	J = 1000 Kg-m2

REFERENCES

[1] Brahim Nait-kaci, Mamadou L. Doumbia, “Active and Reactive power control of a doubly fed induction generator for wind applications”, IEEE 2009.

[2] Braham Nait-kaci, Mamadou L. Doumbia, “Active and Reactive power control of a doubly fed induction generator for wind applications”, IEEE 2009.

[3] C. Eisenhut, F. Krug, C. Schram and B. Klockl, “Wind Turbine Model for System Simulations. Near Cut-in Wind Speed” IEEE Trans, on Energy Conversion, June 2007, vol. 22, 41 4-420.

[4] T.K.A. Brekken “A Novel Control Scheme for a Doubly-Fed Induction Wind Generator under Unbalanced Grid Voltage Condition.” 2005.

[5] B. Shen, B. Mwinyiwiwa, Y. Zhang, and B. –T. Ooi, “Sensorless Maximum Power Point Tracking of Wind by DFIG Using Rotor Position Phase Lock Loop (PLL),” IEEE Transactions on Power Electronics, Vol. 24, no. 4, pp. 942 – 951, Apr. 2009 [6] B. Shen, B. Mwinyiwiwa, Y. Zhang, and B. –T. Ooi, “Sensorless Maximum Power Point Tracking of Wind by DFIG Using Rotor Position Phase Lock Loop (PLL),” IEEE Transactions on Power Electronics, Vol. 24, no. 4, pp. 942 – 951, Apr. 2009.

[7] C. Elmas, , O. Ustun, H. H. Sayan, A neuro-fuzzy controller for speed control of a permanent magnet synchronous motor drive.. Expert Systems with Applications, Vol. 34. n°1, 2008, pp. 657- 664.

[8] C. Elmas, , O. Ustun, H. H. Sayan, A neuro-fuzzy controller for speed control of a permanent magnet synchronous motor drive.. Expert Systems with Applications, Vol. 34. n°1, 2008, pp. 657- 664.

[9] M. Gökbulut, B. Dandil, C. Bal,A hybrid neuro-fuzzy controller for brushless DC motors.
Lecture Notes in Computer Science, 3949, 2006, pp. 125-132.

[10] Runkler. T.A, “Selection of appropriate defuzzification methods using application specific properties”, IEEE Transactions on Fuzzy Systems, 5, 72–79, 1997 [11] Runkler. T.A, “Selection of appropriate defuzzification methods using application specific properties”, *IEEE Transactions on Fuzzy Systems*, 5, 72–79, 1997.

[12] Abdel Karim Guediri1, D. Ben Attous2, "Modeling and fuzzy control of a wind energy system based on double-fed asynchronous machine for supply of power to the electrical network”, The Society for Reliability Engineering, Quality and Operations Management (SREQOM), India and The Division of Operation and Maintenance, Lulea University of Technology, Sweden 2015.

[13] Takagi, T.; Sugeno, M., "Derivation of fuzzy control rules from human operator's control actions," in *Proc. IFAC Symp. On Fuzzy Information, Knowledge Representation and Decision Analysis*, July 1983, pp. 55-60.